Int. J. Electrochem. Sci., 16 **(2021)** Article Number: 21128, doi: 10.20964/2021.12.03

International Journal of
ELECTROCHEMICAL
SCIENCE
www.electrochemsci.org

Enhanced Photocatalytic Performance of Anodized TiO_2 Nanotube Arrays Decorated with $BiVO_4$ Nanoparticles and Its Application for Rhodamine B Degradation

Yu-Long Xie[*], *Cuo-Ji Ben, Li-Fang Guo*

Key Laboratory of Resource Chemistry and Eco-environmental Protection in Tibetan Plateau of State Ethnic Affairs Commission, School of Chemistry and Chemical Engineering, Qinghai Minzu University, Xining, Qinghai, 810007, China
[*]E-mail: yulongxie2012@126.com

Received: 14 July 2021 / *Accepted:* 21 September 2021 / *Published:* 10 November 2021

In this paper, we used the successive ionic layer adsorption and reaction (SILAR) method, and the $BiVO_4$ nanoparticles were successfully deposited on the surface of TiO_2 nanotube arrays (NTs). The coupling of $BiVO_4$ and TiO_2 NTs significantly improved the photocatalytic activity of Rhodamine B (RhB) degradation by visible light. The prepared heterostructured $BiVO_4/TiO_2$ NTs photocatalysts were characterized by field emission scanning microscope (FE-SEM), X-ray diffraction (XRD), UV-Vis diffuse reflectance spectroscopy, transient photocurrent responses. The prepared $BiVO_4/TiO_2$ NTs-7 showed the significantly improved photocatalytic activity for the degradation of RhB. This excellent photocatalytic performance is attributed to the enhancement of visible light absorption and separation efficiency of photogenerated charge carriers on heterostructured $BiVO_4/TiO_2$ NTs. This simple method could be able to utilize in the preparation of high-performance heterostructures for environmental photocatalytic, sensing, and photo-voltaic applications.

Keywords: TiO_2 nanotube arrays, $BiVO_4$, Photocatalytic, Photoelectrochemical performance

1. INTRODUCTION

In the past few decades, photocatalysis has attracted increasing attention for its environmental and energy applications [1, 2]. Semiconductor photocatalyst is considered as a promising material to solve the problem of energy shortage and environmental pollution because of the excellent photocatalytic (and/or electrochemical) activity [3-6]. As we all know, the n-type semiconductor of TiO_2 has the advantages of unique, low cost, good stability, acid resistance, non-toxic and favorable band edge positions [7, 8], which has been used in photocatalyst and electrochemical electrode. The TiO_2

nanoparticles are attractive photocatalysts in industrial waste water purification and novel energy development, and many research papers about TiO_2 photocatalysis have been reported in this year [9-12]. Although TiO_2 is a good photocatalyst, it cannot be effectively used under visible light because it is only absorbs ultraviolet light no longer than 387.5 nm because of the band gap of 3.2 eV, which only occupies about 4% of sunlight [13]. So as to enhance its photocatalytic properties, bismuth oxyhalide composites, such as $BiVO_4/TiO_2$ [14], BiOCl/BiOI [15], $BiOI/TiO_2$ [16, 17], Pd/BiOCl/BiOI [18], $BiVO_4$/BiOI [19], CdS/WO_3/BiOI [20], and BiOI/NiO [21] composites have been prepared, and its photocatalytic performance showed higher than that of its original form. Thus the high-active semiconductors with narrow band gaps could help TiO_2 photocatalyst improve the visible light absorption, and it also simultaneously provides effective electron transportation path, which dramatically reduces the recombination of photoelectrons [22-26].

In this respect, $BiVO_4$ is one of the new materials that have been recognized as a photocatalyst driven by visible light. However, the fast charge recombination and low conductivity of $BiVO_4$ lead to low photocatalytic degradation rate [27, 28]. So as to improve the electron transfer property of $BiVO_4$, many means have been studied, such as structural design, heterojunctions and doping [29-32]. Unusually, coupling $BiVO_4$ with TiO_2 exhibit better charge separation and attractive photocatalytic performance [33-37] on the degradation of organic pollutants by visible light irradiation.

The TiO_2 nanotube arrays (TiO_2 NTs) prepared on Ti substrate [38] have higher specific surface area and highly ordered tubular structures, showing superior photocatalytic and photoelectronic properties compared with TiO_2 powders. Dai et al. [39] reported $BiOI/TiO_2$ NTs heterojunction, and the $BiOI/TiO_2$ NTs samples showed the higher visible light absorption, photocurrent response and significantly enhanced photoelectrocatalytic activity for the degradation of MO dyes. Liu et al. [6] reported TiO_2 NTs decorated with BiOI as an enhanced photocatalyst for degradation of organic pollutants under visible light irradiation. Liu et al. [40] reported $BiOI/TiO_2$ NTs p–n junctions by loading BiOI nanoflakes on TiO_2 NTs walls, and the as-prepared $BiOI/TiO_2$ NTs samples showed the high visible-light photocurrent response and PEC activity. Therefore, the effective electron transportation along the vertical walls of TiO_2 NTs will significantly reduce the recombination of electron/hole pairs in BiOI. The prepared $BiOI/TiO_2$ NTs nanocomposite was effffectively used for water treatment by visible-light irradiation. However, the deposition of $BiVO_4$ on TiO_2 NTs to further improve the photocatalytic efficiency is rarely studied. In this paper, $BiVO_4$ nanoparticles were prepared on the surface of TiO_2 NTs by the successive ionic layer adsorption and reaction (SILAR) deposition method. The $BiVO_4/TiO_2$ NTs photoelectrode exhibited superior photocatalytic and photoelectronic performances. The high photoelectric activity and simple synthesis of $BiVO_4/TiO_2$ NTs would provide the template for the preparation and application of $BiVO_4/TiO_2$ NTs. And the results showed that the $BiVO_4/TiO_2$ NTs nanocomposite exhibited more efficient photocatalytic activity than pure TiO_2 NTs.

2. EXPERIMENTAL

TiO_2 NTs were prepared by anodization of Ti foils (99.9% purity) with a thickness of 250 μm in a two-electrode cell of 2.0 vol.% H_2O and 0.3 wt% NH_4F in ethylene glycol. $BiVO_4$ nanoparticles were

deposited on the surface of TiO_2 NTs by the SILAR method. Initially, TiO_2 NTs were immersed in 3 $mmol \cdot L^{-1}$ $Bi(NO_3)_3 \cdot 5H_2O$ solution for 30 s. After that, the samples were washed with deionized water, and then immersed in 3 $mmol \cdot L^{-1}$ NH_4VO_3 solution for 1 min, and washed again with deionized water. After several cycles of this step, $BiVO_4/TiO_2$ NTS nanocomposites were successfully prepared. The samples prepared after 3, 7 and 12 cycles were labeled as $BiVO_4/TiO_2$ NTs-3, $BiVO_4/TiO_2$ NTs-7, $BiVO_4/TiO_2$ NTs-12. Finally, prepared $BiVO_4/TiO_2$ NTs nanocomposites were calcined for 2 h at 300 °C in air.

The samples were illuminated with a solar simulator equipped with a 500 W Xe lamp (CELS500) with a visible-light filter (≥420 nm). The dye concentration was determined with a UV-VIS-NIR spectrophotometer by detecting the maximum absorption wavelengths for RhB at 552 nm. The electrochemical properties of $BiVO_4/TiO_2$ NTs nanocomposites were investigated in 0.5 M Na_2SO_4 solution using a typical three-electrode system with the CHI 660E electrochemical workstation at room temperature. The prepared samples was regarded as working electrode, and Ag/AgCl and Pt served as the reference and counter electrodes, respectively.

The X-ray diffraction (XRD) patterns of samples were characterized using a diffractometer (Vltima IV, Rigaku). The morphologies of samples were examined by a field emission scanning microscope (FE-SEM, Sigma 500, Carl Zeiss, Germany). The optical absorption of the as-prepared samples was investigated by the UV-Vis diffuse reflectance spectroscopy on a UV-VIS-NIR spectrophotometer (UV-3600 Plus, SHIMADZU) using $BaSO_4$ as the reference. The samples were illuminated with a 150 W Xe lamp solar simulator. The photochemical properties of $BiVO_4/TiO_2$ NTS nanocomposites were investigated in 0.5 M Na_2SO_4 solution using a typical three-electrode system with the CHI 660E electrochemical workstation at room temperature. The dye concentration was determined with a UV-VIS-NIR spectrophotometer UV-3600 Plus, SHIMADZU) by detecting the maximum absorption wavelengths for RhB at 552 nm.

3. RESULTS AND DISCUSSION

Fig. 1 shows the FE-SEM images of pure TiO_2 NTs and the $BiVO_4/TiO_2$ NTs-7 samples. Fig. 1(a) and inset image clearly shows the uniform arrays of TiO_2 NTs, and all tubes are perpendicular to the titanium substrate. The magnified image (Fig. 1(a) inset) shows that the TiO_2 NTs are well opened at the top with a uniform wall thickness of about 15 nm and an inter-pore diameter about 130 nm. Fig. 1(b) and inset shows the morphology and microstructure of the $BiVO_4/TiO_2$ NTs-7 nanocomposites after the deposited $BiVO_4$ nanoparticles on the surface of TiO_2 NTs by the SILAR method.

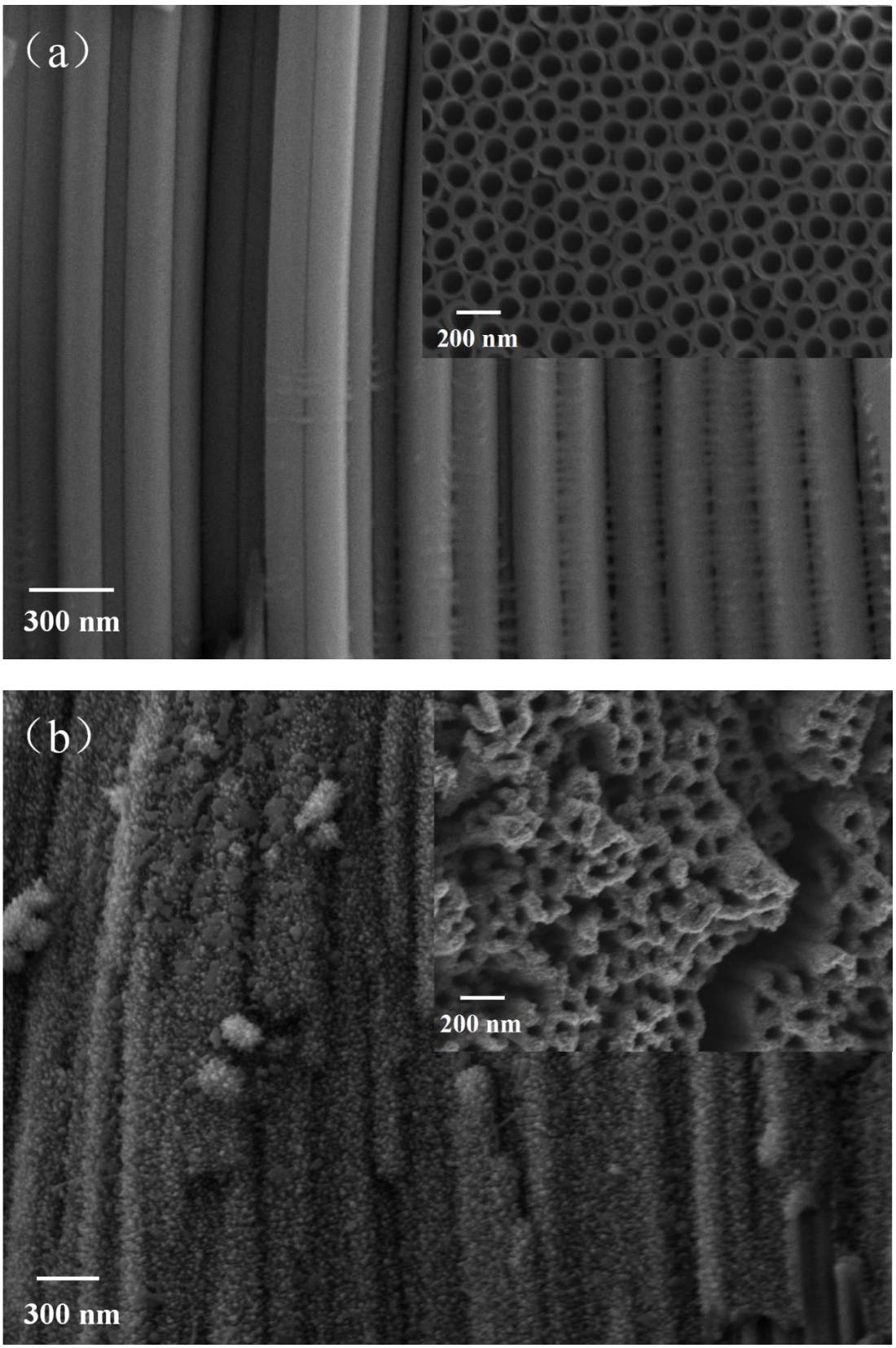

Figure 1. (a) SEM image of TiO_2 NTs, (b) SEM image of $BiVO_4/TiO_2$ NTs-7.

As Fig. 1(b) exhibits that, after the deposited $BiVO_4$ nanoparticles, TiO_2 NTs were transformed into a coaxial structure. The $BiVO_4$ nanoparticles were deposited on the TiO_2 NTs. From the top view (Fig. 1(b) inset) and the side view (Fig. 1(b)), it can be seen that the pores of TiO_2 NTs are still open and the deposited $BiVO_4$ nanoparticle layer is uniform, indicating that the $BiVO_4$ nanoparticle layer is growing along the inner wall surface of TiO_2 NTs. We can see from the Fig. 1(b), the $BiVO_4$ layer is composed of very small $BiVO_4$ nanoparticles, resulting in a rough and porous inner layer. The inner surface of $BiVO_4/TiO_2$ NTs-7 is rough, which is advantageous to dye adsorption and photocatalysis.

We further confirmed the X-ray powder diffraction (XRD) studies of the product (Fig. 2), in which the diffraction peaks of $BiVO_4/TiO_2$ NTs-7 are assigned to mixture phase of $BiVO_4$ and anatase TiO_2. The $BiVO_4/TiO_2$ NTs-7 samples displayed diffraction peaks, which could be indexed to the monoclinic scheelite phase of $BiVO_4$, the additional peaks are the same as that of anatase TiO_2. After deposition of $BiVO_4$ on TiO_2 NTs, the new peaks are observed in addition to the diffraction peaks from the TiO_2 NTs.

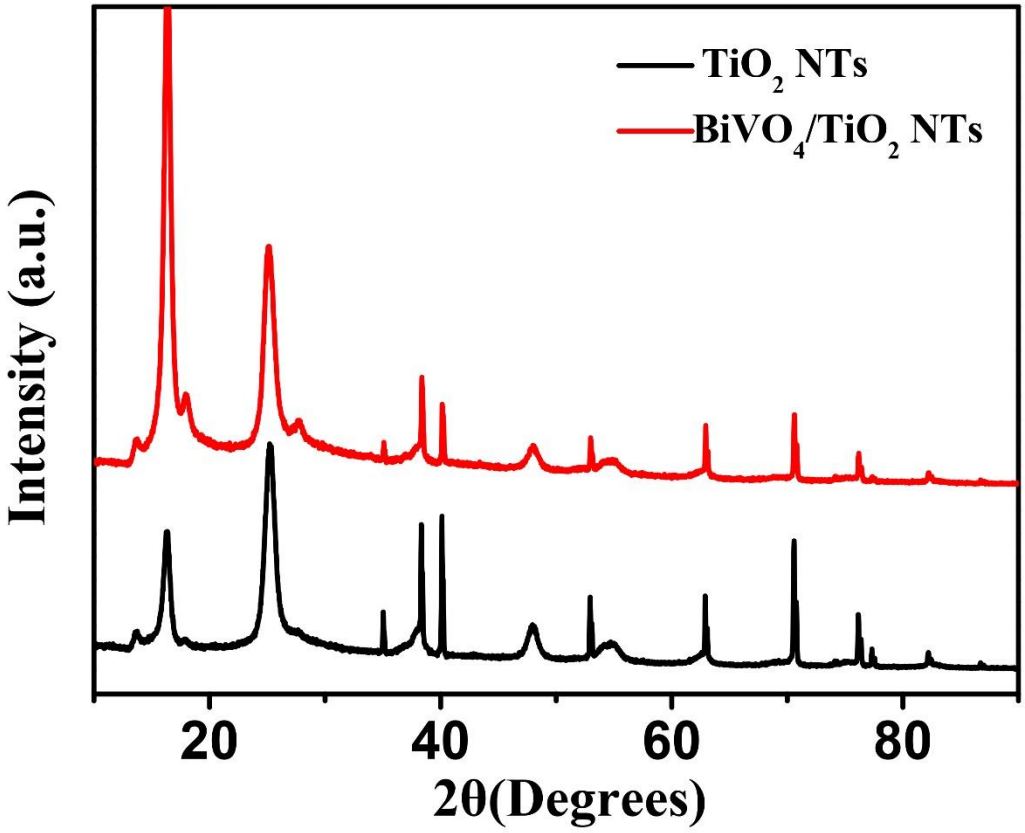

Figure 2. XRD patterns of TiO_2 NTs and $BiVO_4/TiO_2$ NTs-7.

Fig. 3(a) shows that the UV–vis absorption spectra of the pure TiO_2 NTs and the $BiVO_4/TiO_2$ NTs. In Fig. 3(a), the pure TiO_2 NTs had high absorption in the UV region but lower absorption in visible light region. Compared with absorption of TiO_2 NTs, all the $BiVO_4/TiO_2$ NTs heterojunction show a significant enhancement in the visible light region. The optical absorption edge red-shift along with the

increase of $BiVO_4$ deposition cycles, which shows that the $BiVO_4$ addition led to absorption increase in visible region. Obviously, the $BiVO_4/TiO_2$ NTs prepared by SILAR method resulted in the shift of the absorbance region toward longer wavelength. The $BiVO_4/TiO_2$ NTs samples have higher visible light absorbance, which may be due to the presence of $BiVO_4$ in the composites, and makes the composites have higher photoactivity under visible light. It could be seen clearly that the $BiVO_4/TiO_2$ NTs-7 showed the highest efficiency of visible light absorption performance. However, with the increase of $BiVO_4$ deposition cycles, the $BiVO_4/TiO_2$ NTs-12 exhibited lower visible light response. The reason could be attributed to the visible light reflected at the surface of too much $BiVO_4$ nanoparticle layer on top of the coaxial $BiVO_4/TiO_2$ NTs in $BiVO_4/TiO_2$ NTs-12 sample, but the coaxial $BiVO_4/TiO_2$ NTs microstructures could achieve multiple reflections. Under solar/visible light irradiation, $BiVO_4$ is easily excited due to the narrow band gap, generating massive electron-hole pairs. The energy bands of $BiVO_4$ and TiO_2 NTs are well matched to form stable heterojunctions. The redox capacity of photogenerated electrons and holes depends on the conduction/valence band potentials of semiconductors [41-43]. Consequently, the high visible light response of $BiVO_4/TiO_2$ NTs-7 with coaxial $BiVO_4/TiO_2$ NTs structures displayed the highest solar absorption, which would lay the foundations for the photoelectric conversion and significantly enhanced photoelectrocatalytic degradation of organic pollutants.

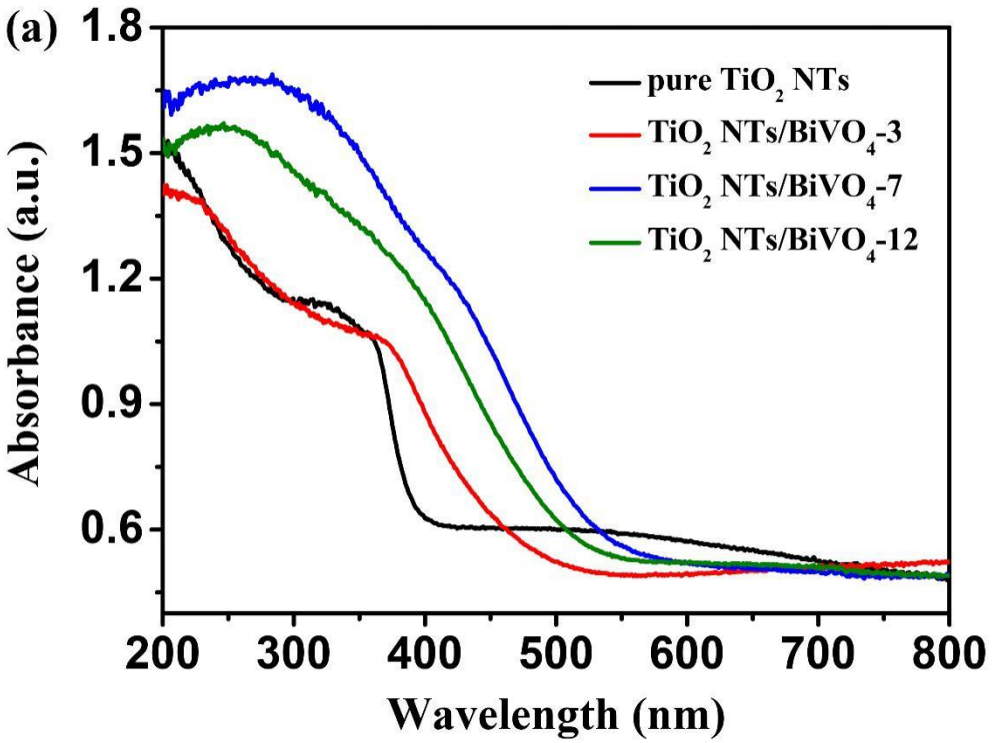

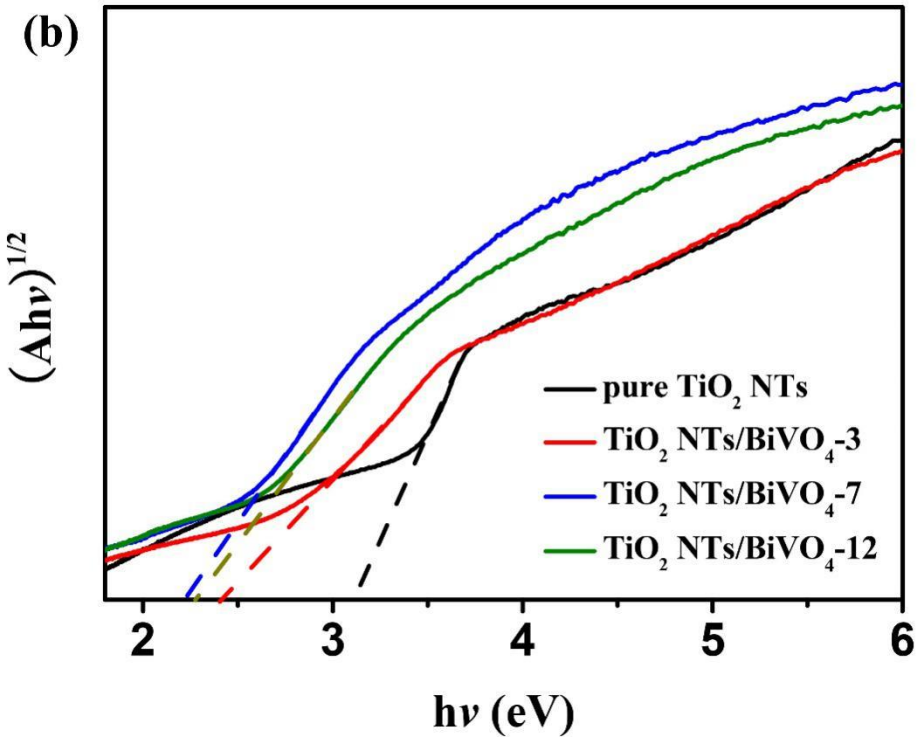

Figure 3. (a) UV-vis diffuse reflectance spectra, (b) band gap energy of samples.

Fig. 3(b) shows band gap value (E_g) of samples. The band gap value (E_g) of a semiconductor can be estimated through the following equation:

$$\alpha h\nu = A(h\nu - E_g)^{n/2} \quad (1)$$

where α is the absorption coefficient, h is Planck's constant, ν is the frequency of the light, A is proportionality constant, and E_g is band gap. The band gap values of TiO_2 NTs, $BiVO_4/TiO_2$ NTs-3, $BiVO_4/TiO_2$ NTs-7, and $BiVO_4/TiO_2$ NTs-12 are calculated to be 3.12, 2.43, 2.25, and 2.28 eV, respectively.

In order to provide a sensible interpretation for the improved photocatalytic activity of $BiVO_4/TiO_2$ NTs heterostructure photocatalysts, photoelectrochemistry properties of TiO_2 NTs, $BiVO_4/TiO_2$ NTs-3, $BiVO_4/TiO_2$ NTs-7, and $BiVO_4/TiO_2$ NTs-12 heterostructure have been studied as photoanodes. Fig. 4 shows the recombination rate and transfer of the photoexcited electrons and holes through the photocurrent response. It is obvious that $BiVO_4/TiO_2$ NTs composites displays stronger photocurrent compared with TiO_2 NTs under visible light irradiation, and $BiVO_4/TiO_2$ NTs-7 evidently demonstrates the highest photocurrent density. The excellent photoelectric conversion characterization means that as-prepared photoelectrodes have strong visible light response, long carrier lifetime and low recombination ratio [41, 44].

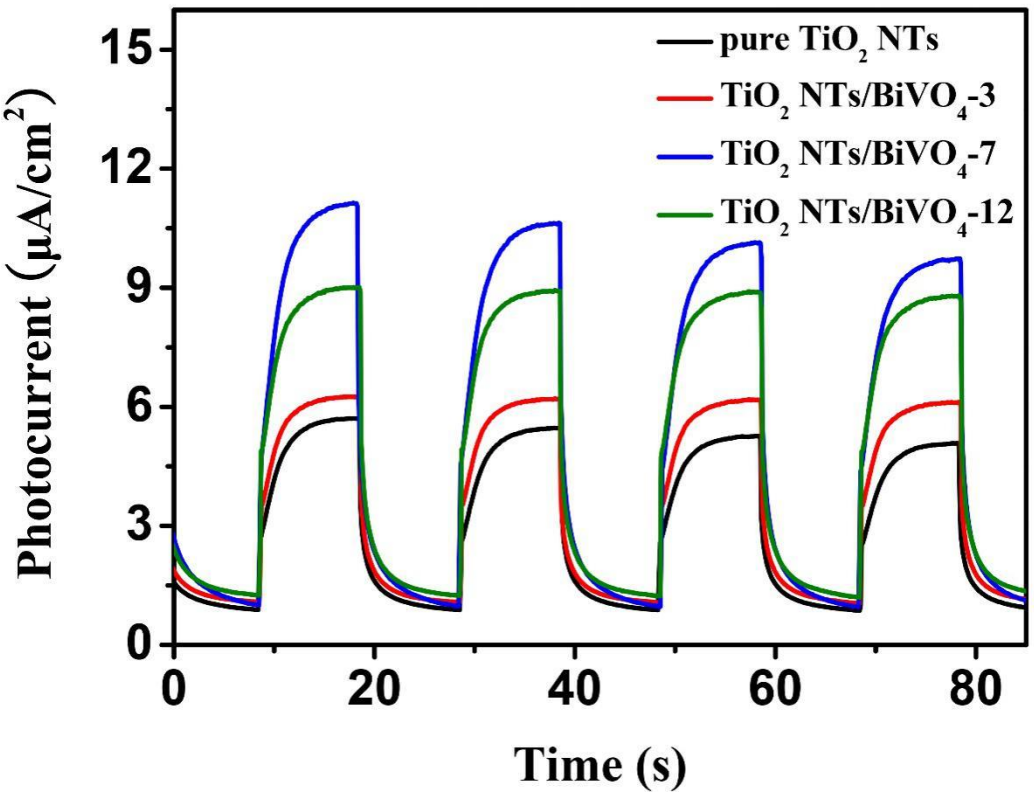

Figure 4. Transient photocurrent responses of samples (the prepared samples was regarded as working electrode, and Ag/AgCl and Pt served as the reference and counter electrodes in 0.5 M Na_2SO_4 solution).

These results indicate that the formation of $BiVO_4/TiO_2$ NTS heterojunction improves the separation efficiency of photogenerated carriers, leading to the promoted photocatalytic activity. As we can see clearly from the Fig. 4, the $BiVO_4/TiO_2$ NTs prepared by SILAR method resulted in the increase of the photocurrent. Higher photocurrent of $BiVO_4/TiO_2$ NTs sample may be due to presence of $BiVO_4$ in the composites, which makes these composites have higher photoactive under visible light. It could be seen clearly that the $BiVO_4/TiO_2$ NTs-7 showed the highest efficiency of photoelectric transformation. However, as the $BiVO_4$ deposition cycle increases further, $BiVO_4/TiO_2$ NTs-12 showed low photocurrent response. The reason could be attributed to the visible light reflected from the surface of too much $BiVO_4$ nanoparticles layer on top of the coaxial $BiVO_4/TiO_2$ NTs in $BiVO_4/TiO_2$ NTs-12 sample, but the coaxial $BiVO_4/TiO_2$ NTs microstructures could achieve multiple reflections. Thus, the high visible light response of $BiVO_4/TiO_2$ NTs-7 with coaxial $BiVO_4/TiO_2$ NTs structures exhibited the highest photoelectric conversion efficiency, which would lay the foundations for the photoelectric conversion and significantly enhanced photoelectrocatalytic degradation of organic pollutants.

Under the visible light irradiation, the photocatalytic degradation of RhB as a function of time over different photocatalysts is shown in Fig. 5. As was well known, the pure TiO_2 NTs presented incapability for RhB degradation, because it almost cannot absorb visible light. However, the pure $BiVO_4$ has a narrow band gap so that electro and hole would be recovered quickly under visible light

irradiation. The TiO_2 NTs decorated with $BiVO_4$ nanoparticles could overcome these shortcomings. As the samples prepared by SILAR method with the increase of $BiVO_4$ deposition cycles, the $BiVO_4/TiO_2$ NTs-7 shows the highest photocatalytic performance. As the deposition cycles of $BiVO_4$ was increased from 7 to 12, the photocatalytic activity of $BiVO_4/TiO_2$ NTS-12 was decreased. This may be due to the fact that some $BiVO_4$ nanoparticles do not form heterojunction with TiO_2 NTs when $BiVO_4$ nanoparticles are redundant. The superfluous $BiVO_4$ nanoparticle layer on top of the coaxial $BiVO_4/TiO_2$ NTs in $BiVO_4/TiO_2$ NTs-12 samples, but the coaxial $BiVO_4/TiO_2$ NTs microstructures could achieve multiple reflections. Under visible light irradiation, these pure $BiVO_4$ nanoparticles may act as the recombination centers of photogenerated electrons and holes, resulting in a reduced photocatalytic activity.

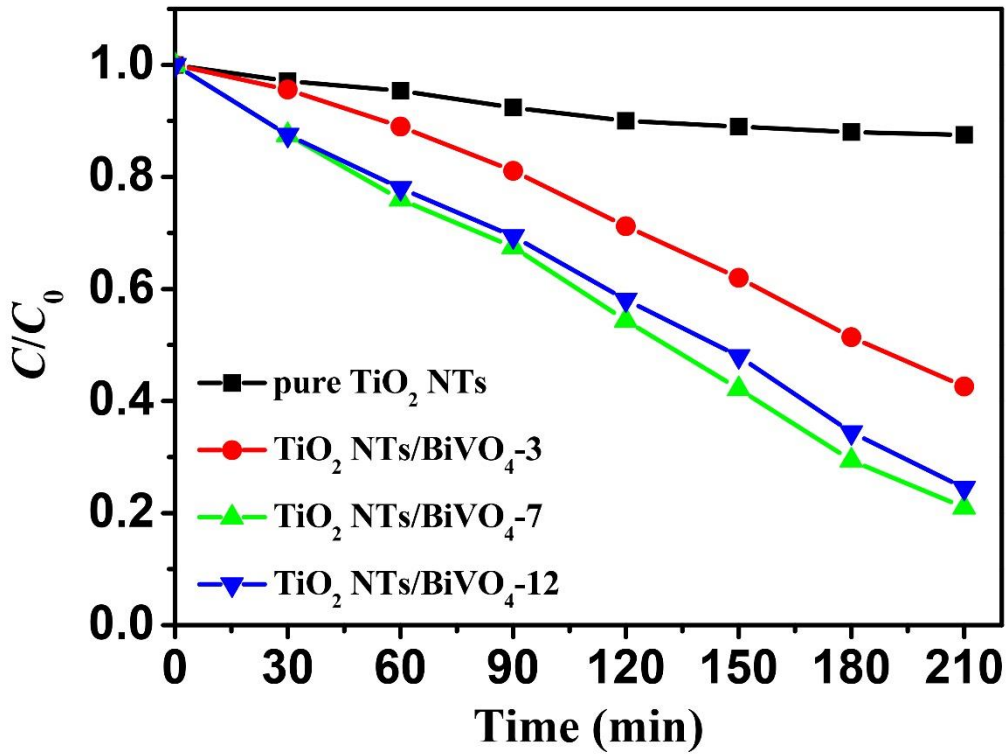

Figure 5. Photocatalytic degradation of RhB with a concentration of 20 mg/L by photocatalyst samples under visible light irradiation.

Therefore, the high visible light response of $BiVO_4/TiO_2$ NTs-7 with coaxial $BiVO_4/TiO_2$ NTs structures exhibited the high solar absorption, which would lay the foundations for the photoelectric conversion and significantly enhanced photoelectrocatalytic degradation of organic pollutants. In particular, $BiVO_4/TiO_2$ NTs-7 displayed the optimal enhanced photoelectrocatalytic degradation of RhB, and the final efficiency reached 70.6% after solar irradiation for 3 h, which reaches to 8 times compared with those of pure TiO_2 NTs. All of $BiVO_4$ loading samples ($BiVO_4/TiO_2$ NTs-3, $BiVO_4/TiO_2$ NTs-7, and $BiVO_4/TiO_2$ NTs-12) can effectively degrade RhB dye under visible light, and is more efficient when used in combination with $BiVO_4/TiO_2$ NT-7. This may be owing to higher visible light absorption

of $BiVO_4/TiO_2$ NTs-7 sample confirmed by UV–vis absorption spectra measurements (Fig. 3) and additionally decrease of electron-hole recombination in $BiVO_4/TiO_2$ NTs heterojunction. Among these samples, $BiVO_4/TiO_2$ NTs-7 is found to be very efficient for RhB degradation under visible light. The table 1 shows the photocatalytic Rhodamine B degradation comparison of TiO_2 NTs-based photocatalysts. The p-n heterojunction construction of TiO_2 NTs-based photocatalysts benefited the solar response, photoelectron separation and photocatalytic reaction.

Table 1 The photocatalytic Rhodamine B degradation comparison of TiO_2 NTs-based photocatalysts.

Photocatalyst	**Preparation method**	**Light source**	**Efficiency**	**Ref.**
TiO_2 NTs/CdS–CuS	hydrothermal deposition	300 W Xe-lamp ($\lambda \geq$ 420 nm)	78.86%	[45]
TiO_2 NTs/BiOI	successive ionic layer adsorption and reaction	500 W Xe-lamp ($\lambda >$ 400 nm)	62%	[6]
TiO_2 NTs/Bi_2MoO_6	solvothermal method	500 W Xe-lamp ($\lambda >$ 400 nm)	75%	[41]
Bi/Bi_2MoO_6/TiO_2 NTs	solvothermal method	500 W Xe-lamp ($\lambda \geq$ 420 nm)	73.21%	[46]
$BiVO_4/TiO_2$ NTs	successive ionic layer adsorption and reaction	500 W Xe-lamp ($\lambda \geq$ 420 nm)	70.6%	This work

Fig. 6 shows the good reusability and stability of the prepared $BiVO_4/TiO_2$ NTs-7 composites in the four cycles. As shown in Fig. 6, the photocatalytic activity of $BiVO_4/TiO_2$ NTS-7 decreased slightly compared with the fresh $BiVO_4/TiO_2$ NTs-7 sample after four cycles of degradation of RhB under visible light irradiation. As a result, $BiVO_4/TiO_2$ NTs-7 could be considered as a highly reusable and stable photocatalyst for degradation of RhB under visible light irradiation. Consequently, the photocatalytic performance of the $BiVO_4/TiO_2$ NTs photocatalysts was greatly improved because of the formation of heterojunction and the enhanced visible light absorption.

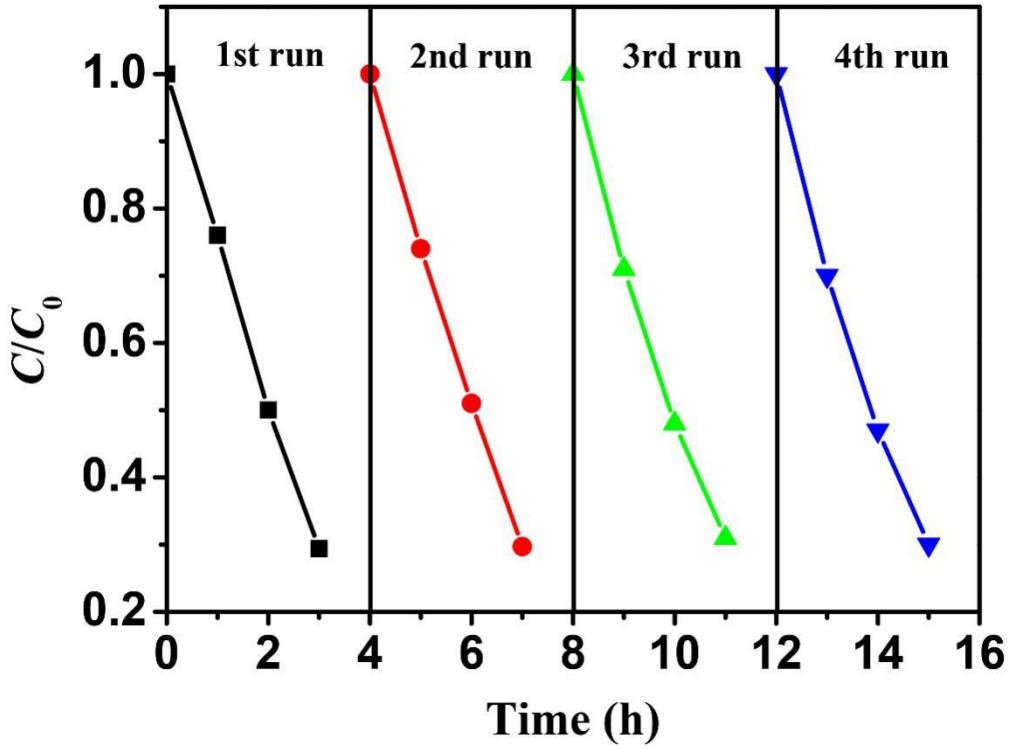

Figure 6. Reusability of TiO_2 NTs/$BiVO_4$-7 for degradation of RhB for 4 consecutive cycles.

4. CONCLUSIONS

In conclusion, the results from our studies confirmed that the heterostructured $BiVO_4/TiO_2$ NTs photocatalysts exhibited high photocatalytic performances of RhB degradation. The heterostructured $BiVO_4/TiO_2$ NTs photocatalysts were prepared by the SILAR method. When the sample prepared with 7 cycles, the photocatalysts demonstrated increasing efficiency for photocatalytic degradation of RhB in comparison with pure TiO_2 NTs. The formation of heterojunction $BiVO_4/TiO_2$ NTs promoted the charge separation, efficient transfers of the photoexcited electron-hole pair, and enhanced the visible light absorption. Thus, the photocatalytic performance was improved. The results indicate that the heterostructured $BiVO_4/TiO_2$ NTs nanocomposite is a promising visible light driven photocatalysts for environmental photocatalysis, photovoltaics, and sensing applications.

ACKNOWLEDGEMENTS
Financial support from the Chunhui project of the Ministry of Education (No. Z2017044).

References

1. J.W. Fu, J.G. Yu, C.J. Jiang, B. Cheng, *Adv. Energy Mater.*, 8 (2018) 1701503.
2. M.S. Zhu, S. Kim, L. Mao, M. Fujitsuka, J.Y. Zhang, X.C. Wang, T. Majima, *J. Am. Chem. Soc.*, 139 (2017) 13234.
3. Y. Zhang, F. Zhang, Z. Yang, H. Xue, D.D. Dionysiou, *J. Catal.*, 344 (2016) 692.
4. Y.H. Zhang, Z.R. Tang, X.Z. Fu, Y.J. Xu, *ACS Nano*, 4 (2010) 7303.

5. Y.Z. Hong, Y.H. Jiang, C.S. Li, W.Q. Fan, X. Yan, M. Yan, W.D. Shi, *Appl. Catal. B-Environ.*, 180 (2016) 663.
6. Z. Liu, Q. Wang, X. Tan, Y. Wang, R. Jin, S. Gao, *Sep. Purif. Technol.*, 215 (2019) 565.
7. B. Damardji, H. Khalaf, L. Duclaux, B. David, *Appl. Clay Sci.*, 45 (2018) 98.
8. P. Mazierski, A. Malankowska, M. Kobylański, M. Diak, M. Kozak, M.J. Winiarski, T. Klimczuk, W. Lisowski, G. Nowaczyk, A. Zaleska-Medynska, *ACS Catal.*, 7 (2017) 2753.
9. M. Motola, R. Zazpe, L. Hromadko, P. Jan, V. Cicmancova, J. Rodriguez-Pereira, S. Hanna, J.M. Macak, *Appl. Surf. Sci.*, 549 (2021) 149306.
10. F. Xu, H. Tan, J. Fan, B. Cheng, J. Yu, J. Xu, *Sol. RRL*, 5 (2021) 2000571.
11. M. Umer, M. Tahir, M.U. Azam, M.M. Jaffar, *Appl. Surf. Sci.*, 463 (2019) 747.
12. T. Abbas, M. Tahir, N.A.S. Amin, *Bull. Chem. React. Eng. Catal.*, 16 (2021) 430.
13. Y. Zhang, S. Park, *J. Solid State Chem.*, 253 (2017) 421.
14. Y.-R. Lv, C.-J. Liu, R.-K. He, X. Li, Y.-H. Xu, *Mater. Res. Bull.*, 117 (2019) 35.
15. X. Su, J. Yang, X. Yu, Y. Zhu, Y. Zhang, *Appl. Surf. Sci.*, 433 (2018) 502.
16. C. Liao, Z. Ma, G. Dong, J. Qiu, *Appl. Surf. Sci.*, 314 (2014) 481.
17. D. Wu, H. Wang, C. Li, J. Xia, X. Song, *Surf. Coat. Technol.*, 258 (2014) 672.
18. L. Ren, D. Zhang, X.Y. Hao, X. Xiao, Y. Jiang, J.Y. Gong, F. Zhang, X. Zhang, Z. Tong, *Mater. Res. Bull.*, 94 (2017) 183.
19. L. Shan, Y. Liu, J. Bi, J. Suriyaprakash, Z. Han, *J. Alloys Compd.*, 721 (2017) 784.
20. L. Yosefi, M. Haghighi, *Appl. Catal. B*, 220 (2018) 367.
21. Q. Han, R. Wang, B. Xing, T. Zhang, M.S. Khan, D. Wu, Q. Wei, *Biosens. Bioelectron.*, 99 (2018) 493.
22. B. Tahir, M. Tahir, *Appl. Surf. Sci.*, 506 (2020) 145034.
23. M. Tahir, M. Siraj, B. Tahir, M. Umer, N. Hajar, A. Othman, *Appl. Surf. Sci.*, 503 (2020) 144344.
24. P. Parnicka, W. Lisowski, T. Klimczuk, J. Łuczak, A. Zak, A. Zaleska-Medynska, *Appl. Catal. B Environ.*, 291 (2021) 120056.
25. N.T. Padmanabhan, N. Thomas, J. Louis, D.T. Mathew, P. Ganguly, H. John, S.C. Pillai, *Chemosphere*, 271 (2021) 129506.
26. M. Mahjoubian, A.S. Naeemi, M. Sheykhan, *Chemosphere*, 263 (2021) 128182.
27. C.W. Siao, H.L. Chen, L.W. Chen, J.L. Chang, T.W. Yeh, C.C. Chen, *J. Colloid Interf. Sci.*, 526 (2018) 322.
28. Q. Yang, J. Huang, J.B. Zhong, J.F. Chen, J.Z. Li, S.Y. Sun, *Curr. Appl. Phys.*, 17 (2017) 1202.
29. J. Di, J.X. Xia, M.X. Ji, B. Wang, S. Yin, H. Xu, Z.G. Chen, H.M. Li, *Langmuir*, 32 (2016) 2075.
30. M. Xie, X. Fu, L. Jing, P. Luan, Y.J. Feng, H.G. Fu, Long-lived, *Adv. Energy Mater.*, 4 (2014) 1300995.
31. X. Song, Y. Li, Z. Wei, S. Ye, D.D. Dionysiou, *Chem. Eng. J.*, 314 (2017) 443.
32. Y. Hu, W. Chen, J. Fu, M.W. Ba, F.Q. Sun, P. Zhang, J.Y. Zou, *Appl. Surf. Sci.*, 436 (2018) 319.
33. M.F.R. Samsudin, S. Sufian, N.M. Mohamed, R. Bashiri, F. Wolfe, R.M. Ramli, *Mater. Lett.*, 211 (2018) 13.
34. G. Odling, N. Robertson, *Chemphyschem*, 17 (2016) 2872.
35. H. Li, H. Yu, X. Quan, S. Chen, H.M. Zhao, *Adv. Funct. Mater.*, 25 (2015) 3074.
36. M. Zalfani, B. van der Schueren, Z.Y. Hu, J.C. Rooke, R. Bourguiga, M. Wu, Y. Li, G. Van Tendeloo, B.L. Su, *J. Mater. Chem. A*, 3 (2015) 21244.
37. Y. Hu, D. Li, Y. Zheng, W. Chen, Y.H. He, Y. Shao, X.Z. Fu, G.C. Xiao, *Appl. Catal. B-Environ.*, 104 (2011) 30.
38. Z.Y. Liu, Q.Y. Wang, W.Q. Rong, R.C. Jin, Y.M. Cui, S.M. Gao, *Sep. Purif. Technol.*, 200 (2018) 191.
39. G.P. Dai, J.G. Yu, G. Liu, *J. Phys. Chem. C*, 115 (2011) 7339.
40. J.Q. Liu, L.L. Ruan, S.B. Adeloju, Y.C. Wu, *Dalton Trans.*, 43 (2014) 1706.
41. Z. Liu, Y. Song, Q. Wang, Y. Jia, X. Tan, X. Du, S. Gao, *J. Colloid Interface Sci.*, 556 (2019) 92.

42. H. Huang, L. Liu, Y. Zhang, N. Tian, J. Alloy. Compd., 619 (2015) 807.
43. H.B. Feng, Y.P. Li, D.M. Luo, G.R. Tan, J.B. Jiang, H.M. Yuan, S.J. Peng, D. Qian, Chinese J. Catal., 37 (2016) 855.
44. J. Zhang, C.L. Shao, X.H. Li, J.Y. Xin, R. Tao, Y.C. Liu, ACS Sustain. Chem. Eng., 6 (2019) 10714.
45. J. Hou, B. Huang, L. Kong, Y. Xie, Y. Liu, M. Chen, Q. Wang, *Ceram. Int.*, https://doi.org/10.1016/j.ceramint.2021.07.268.
46. D. Cao, Q. Wang, Y. Wu, S. Zhu, Y. Jia, R. Wang, *Separ. Purif. Technol.*, 250 (2020) 117132